



HAL
open science

Influence of H₂O, CO₂ and O₂ addition on biomass gasification in entrained flow reactor conditions: Experiments and modelling

Joseph Billaud, Sylvie Valin, Marine Peyrot, Sylvain Salvador

► **To cite this version:**

Joseph Billaud, Sylvie Valin, Marine Peyrot, Sylvain Salvador. Influence of H₂O, CO₂ and O₂ addition on biomass gasification in entrained flow reactor conditions: Experiments and modelling. Fuel, 2016, 166, pp.166-178. 10.1016/j.fuel.2015.10.046 . hal-01609022

HAL Id: hal-01609022

<https://hal.science/hal-01609022>

Submitted on 3 Apr 2018

HAL is a multi-disciplinary open access archive for the deposit and dissemination of scientific research documents, whether they are published or not. The documents may come from teaching and research institutions in France or abroad, or from public or private research centers.

L'archive ouverte pluridisciplinaire **HAL**, est destinée au dépôt et à la diffusion de documents scientifiques de niveau recherche, publiés ou non, émanant des établissements d'enseignement et de recherche français ou étrangers, des laboratoires publics ou privés.

Influence of H₂O, CO₂ and O₂ addition on biomass gasification in entrained flow reactor conditions: Experiments and modelling

Joseph Billaud^{a,b}, Sylvie Valin^{a,*}, Marine Peyrot^a, Sylvain Salvador^b

^aCEA, LITEN, DTBH/SBRT/LTCB, 38054 Grenoble cedex 9, France

^bRAPSODEE, UMR-CNRS 5302, Ecole des Mines d'Albi, 81000 Albi, France

H I G H L I G H T S

- Wood particles were gasified in CO₂, H₂O and O₂ atmospheres.
- H₂O and CO₂ addition decrease char and soot production above 1200 °C.
- O₂ addition lowers char, hydrocarbons, soot and tar formation.
- Experiments were modelled with a 1D-model using detailed chemical scheme.
- Gas, char, tar + soot were satisfactorily simulated in the whole range of conditions.

Keywords:

Biomass
Gasification
Entrained flow reactor
Drop tube reactor
Modelling

A B S T R A C T

Biomass gasification in Entrained Flow Reactor (EFR) is both studied with experiments in a drop tube reactor and modelling with a 1-D model (GASPAR). Operating conditions are chosen thanks to results of a preliminary modelling of an industrial EFR. Influence of addition of steam (0.55 g/g db), carbon dioxide (0.87 g/g db) and oxygen (Equivalent Ratio: 0–0.61) is investigated between 800 and 1400 °C with beech wood particles sieved between 315 and 450 µm as feedstock. The model takes into account pyrolysis reaction, gas phase reaction with a detailed chemical scheme (176 species, 5988 reactions), char gasification by steam and CO₂ and soot formation. H₂O or CO addition has no influence on gasification product yields at 800 and 1000 °C, while at 1200 and 1400 °C the char gasification is significantly enhanced and soot formation is certainly inhibited by OH radical which reacts with soot precursors. The modification of output gas phase composition is mostly due to WGS reaction which reaches thermodynamic equilibrium from about 1200 °C. As expected, O₂ has a significant influence on gas and tar yields through combustion reactions. Char and soot yields decrease as ER increases. The GASPAR model allows a good prediction of gas and char and gives relevant evolution of soot and tar yields on the large majority of conditions studied.

1. Introduction

The world is facing a major energy crisis in the recent years. Fossil fuel energy is the first source of primary energy and we are facing two major issues: the depletion of fossil resources while the world energy demand grows [1], and the climate change, generally attributed to the greenhouse gases emissions directly linked to the fossil fuel usage [2]. To cope up with this challenge, numerous alternative sources of energy are explored. Currently, biomass is the first renewable resource in the world and is well spread across the world. Different biomass conversion processes have been developed and biomass gasification appears to be one of

the most promising processes to produce syngas for power generation or biofuel synthesis.

The Entrained Flow Reactor (EFR) is a well-known technology for coal gasification but it still needs development to be operated with biomass as feedstock. The main advantage of this technology is the high conversion of biomass into syngas with a very low tar content which is particularly appropriate for biofuel synthesis processes. The EFR is characterized by a high operating temperature (~1500 °C), a high pressure (>30 bar), a short particle residence time (~5 s) and a high heat flux at particle surface (>1 GW m⁻²). It is generally operated as an autothermal reactor which means that a part of biomass is burnt to supply enough energy for endothermic gasification reactions. Biomass is injected as small particles (smaller than 300 µm).

* Corresponding author.

E-mail address: sylvie.valin@cea.fr (S. Valin).

Nomenclature

A_i	Arrhenius pre-exponential coefficient of i (s^{-1})
C_p	molar calorific capacity of ($kJ\ mol^{-1}\ K^{-1}$)
C_d	drag coefficient (-)
d_{es}	particle equivalent spherical diameter (m)
Ea_i	Arrhenius activation Energy of i ($J\ mol^{-1}$)
ER	Equivalent Ratio
g	standard gravity ($m\ s^{-2}$)
k	Arrhenius law
m_i	mass of i (g)
n_i	Arrhenius order of i (-)
P_i	pressure of i (bar)
P_{loss}	power loss (kW)
Q_i	molar flowrate of i ($mol\ s^{-1}$)
R	perfect gas constant ($J\ mol^{-1}\ K^{-1}$)
Re_p	particle Reynolds Number (-)

T	temperature (K)
t	time (s)
u_{slip}	velocity slip of particle ($m\ s^{-1}$)
X	gasification progress (-)

Greek symbols

α_i	pyrolysis coefficient of i (from experiments) (-)
β_i	pyrolysis coefficient of i (modified) (-)
γ	char coefficient in pyrolysis reaction (-)
ΔH_f^0	formation Enthalpy ($kJ\ mol^{-1}$)
ρ_g	gas volumetric mass ($kg\ m^{-3}$)
ρ_p	particle volumetric mass ($kg\ m^{-3}$)
θ	ash ratio (-)
η_i	yield of i (g of i /g db)

In order to improve the knowledge on this technology, experimental and modelling studies have been conducted. Experimental ones are generally performed with lab-scale reactors which allow reproducing some important EFR characteristics as temperature, heat flux, residence time and particle size: the Drop Tube Reactor (DTR). Only few studies have dealt with woody biomass pyrolysis in a DTR above 1000 °C [3–6]. Woody biomass gasification has been studied at high temperature ($T > 1000\ ^\circ C$) in presence of oxygen [4,7,8] and/or in presence of steam [4,7,9–11] or in presence of carbon dioxide [11]. These studies show a high influence of gasification atmosphere both on carbon conversion and on the product gas composition. Recently, several biomass EFR pilot facilities have been built to study biomass gasification in conditions close to those of an industrial plant [12,13].

In parallel, gasification models using equilibrium model [12] or CFD calculations [14] have been developed and tested. These models, which include simple reaction schemes, generally allow predicting the syngas composition with a good accuracy for the main gases (CO , H_2 , CO_2 , CH_4 , H_2O) but are unable to predict tar and soot production. On the other hand, detailed chemical schemes based on elementary reactions are able to predict the production of minor products [15,16] and are very useful to better understand the mechanisms leading to undesirable products like soot or tars. These detailed chemical schemes have rarely been integrated into biomass gasification reactor models and validated with experimental results [17,18].

The present study aims to investigate wood particle conversion in a DTR between 800 °C and 1400 °C, both with experiments and simulations. Experiments were conducted in inert and in oxidizing atmospheres with beech wood particles as feedstock. The oxidizing atmospheres included: oxygen which is necessary to heat an autothermal reactor, steam which could be added to improve biomass gasification and carbon dioxide which could be recycled from the reactor output to be used as carrier gas. The amounts of oxygen, steam or carbon dioxide injected were chosen to be representative of an EFR. An existing model [10] was improved to represent biomass particle conversion in presence of these oxidants and was validated by comparison with the experimental results.

2. Materials and methods

2.1. Feedstock

The feedstock used for the experiments is beech sawdust sieved in a size range of 0.315–0.450 mm. The proximate analysis and the ultimate analysis are given in Table 1.

Table 1

Proximate and ultimate analyses of beech sawdust.

Proximate analysis	
Moisture (wt%)	8.7
Volatile matter (wt% db)	84.3
Fixed carbon ^a (wt% db)	15.2
Ash (550 °C) (wt% db)	0.80
Ash (815 °C) (wt% db)	0.46
Ultimate analysis (wt% db)	
C	49.1
H	5.7
N	<0.3
S	0.0453
O ^a	44.5

^a Calculated by difference.

2.2. The drop tube reactor

Experiments were conducted in a Drop Tube Reactor (DTR) presented in Fig. 1. It consists of an alumina tube inserted in a vertical electrical heater with three independent heating zones. The internal diameter of the tube is 0.075 m and the heated zone length is 1.2 m. The DTR works at atmospheric pressure and can reach a maximum temperature of 1400 °C.

The wood particles are continuously fed into the reactor using a gravimetric feeding system, controlled by a computer enabling a $\pm 1\%$ accuracy for the flowrate. The wood particles are entrained to a pneumatic ejector from which they are injected into the reactor with a $1.5\ NL\ min^{-1}$ transport nitrogen stream through a water-cooled (30 °C) feeding probe. A dispersion dome is placed at the outlet of the feeding probe to distribute the solid particles over the reactor cross section.

The main gas stream, which can be N_2 or a mixture of N_2 and H_2O , air or CO_2 is electrically pre-heated before entering the reactor. For the introduction of H_2O into the DTR, a steam generator working at 180 °C is set at the reactor inlet.

An oil-cooled (110 °C) sampling probe can be inserted at different heights in the bottom half of the reactor to collect gas and the remaining solid. A fraction of the exhaust gas is sucked in the sampling probe and passes through a settling box and a filter or in a tar protocol if tars are sampled. This part of the experimental facility is heated (150 °C) to avoid steam condensation. After the filter, the sampled gas passes through a condenser if steam is introduced into the reactor, and is finally analyzed.

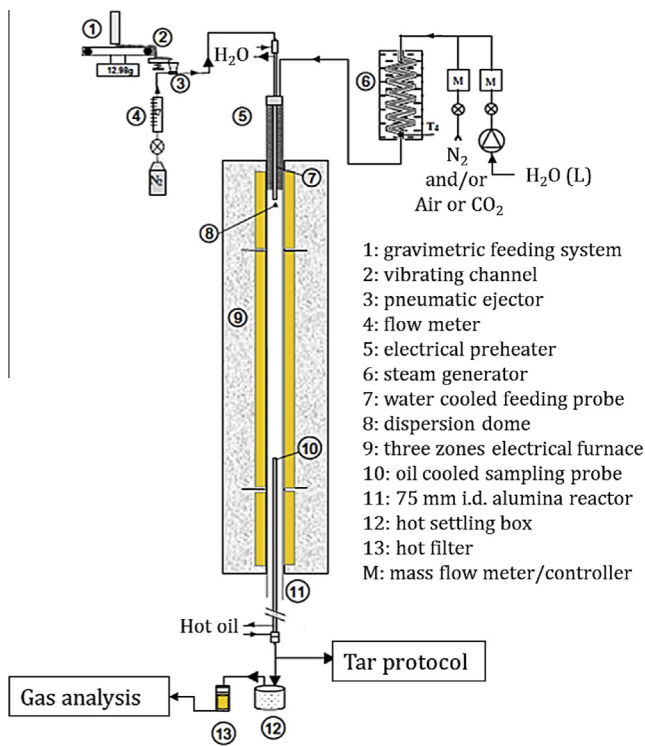


Fig. 1. Scheme of the drop tube reactor.

2.3. Gas analysis

Main gaseous compounds are analyzed online with a micro-gas chromatograph (H_2 , CO , CO_2 , CH_4 , C_2H_2 , C_2H_4 , C_2H_6 , C_3H_8 , C_6H_6 , O_2 and N_2), a psychrometer (H_2O), a paramagnetic detector (O_2), a Thermal Conductivity Detector (H_2) and a Non-Dispersive Infrared Spectrometer (CO_2). Three different columns are settled in the micro-gas chromatograph: H_2 , O_2 , N_2 , CO and CH_4 are analyzed using a molsieve 5A; CO_2 , C_2H_4 , C_2H_6 , C_2H_2 and C_3H_8 are analyzed using a Propyl-pyridyl-urea column (PPU) connected to a back flush inlet. At last, a non-polar dimethylsilicone capillary column (OV1) is used to measure C_6H_6 concentration.

Gas yields are calculated using the tracer method with N_2 as tracer. Repeatability of these experiments was checked at several days and months of interval; the relative difference between experiments is inferior to 15% in most cases but for some species in some conditions repeatability is not as good. In Section 3, the experimental results are not given as mean values but all repeatability experiments results are plotted. The experimental relative uncertainties on gas yields are estimated at about 10% for CO , CO_2 , H_2 , CH_4 and 15% for C_2H_2 , C_6H_6 , C_2H_4 , C_2H_6 , C_3H_8 and steam.

2.4. Tar sampling and analysis

A part of the product gas stream containing tar is continuously sucked and passed through a sampling train composed of a filter, five Erlenmeyer flasks filled with isopropanol – three in a “hot” bath at $40^\circ C$ and two in a “cold” bath at $-70^\circ C$ made with a mixture of isopropanol and carbon ice, a pump and a volumetric gas counter. Each tar sampling lasts about 30 min at a flow rate of 2 NL min^{-1} .

Isopropanol samples are analyzed using a gas chromatographer connected to a Flame Ionization Detector (GC-FID). Knowing the volume of gas passing through the tar protocol, the time of

sampling and the concentration of tars in each Erlenmeyer flasks, the tar yields can be deduced. Tar analyses were only performed for experiments at $800^\circ C$ in pyrolysis conditions defined in Table 3.

2.5. Solid residue analysis

Char and soot are both collected in the settling box and the filter after each experiment. Char is mainly retained in the settling box whereas soot is mainly in the filter. This segregation phenomenon has been previously observed [6].

Char yield is calculated thanks to the ash tracer method. The ash contents of initial biomass and of chars are measured at $815^\circ C$. Considering that ash totally remains in the char, the char yield can be calculated according to the following equation:

$$\eta_{\text{char}} = \frac{\theta_{\text{biomass}}}{\theta_{\text{char}}} \quad (1)$$

with η_{char} , the char yield and θ_{char} and θ_{biomass} , the ash contents in char and biomass respectively.

Note that this ash tracer method was validated with other furnaces in pyrolysis conditions at $800^\circ C$ and $1100^\circ C$. The char yield was determined by weighing on the one hand, and by the ash tracer method on the other hand. The relative error between the two measurements was about 3%.

Two different protocols were used to measure the ash content in char:

- If the available mass of char was superior to 300 mg, a laboratory furnace was used following the ISO 1171: 2010 standard. The minimal char quantity for the ash content measurement was 300 mg.
- If the available mass was under 300 mg, the ash content was measured with a Thermo Gravimetric Analyser (TGA), following the same temperature history as in the laboratory furnace. The required mass of char was about 10 mg. This protocol was validated by comparison with the first one and the maximal relative difference was 5%.

C and H contents in chars were also measured with a microanalyser when the remaining quantities of chars were sufficient ($m_{\text{char}} > 50\text{ mg}$). The relative uncertainty was calculated for each char yield measurement and ranges between 5% and 15%.

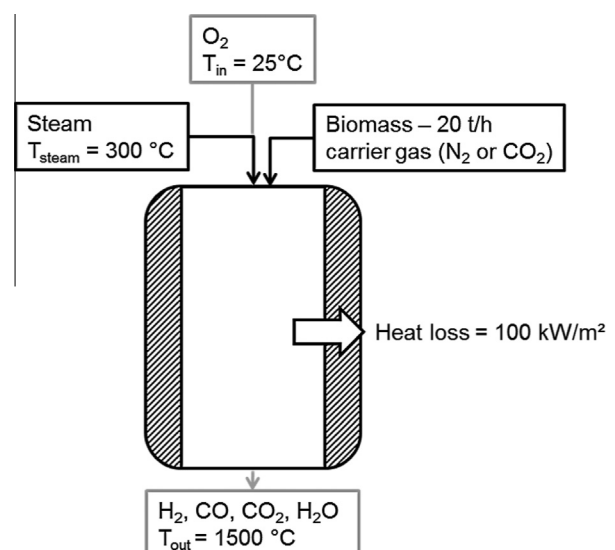


Fig. 2. Input data and assumptions for the EFR modelling.

Table 2Calculated ER as a function of S/B with N₂ or CO₂ as carrier gas.

	Carrier gas					
	N ₂ = 0.28 g/g db			CO ₂ = 0.44 g/g db		
Steam/biomass (g/g db)	0	0.27	0.64	0	0.27	0.64
Steam content (vol%)	0%	33.6%	53.1%	0%	33.0%	52.5%
ER	0.43	0.46	0.51	0.45	0.48	0.53
O ₂ content (vol%)	63.7%	43.5%	31.8%	64.8%	44.5%	32.6%

2.6. Experimental conditions

2.6.1. Experimental conditions determination

In order to choose relevant conditions for our experimental study, an autothermal full scale EFR was modelled (Fig. 2) with simple assumptions. Thermodynamic equilibrium was assumed at the output of the reactor (Gibbs Energy minimization) at a temperature of 1500 °C and a pressure of 40 bar. The gas residence time was assumed to be about 4 s which allowed sizing the EFR: length = 4.1 m and diameter = 1.6 m. In the pressurized biomass feeding line at 25 °C, the wood particle volume concentration and density were considered to be 20 vol% and 650 kg/m³ respectively. Heat loss was estimated at 100 kW m⁻² of internal surface. The biomass specifications are those of the beech sawdust used for the drop tube reactor experiments (Table 1).

The energy balance of the reactor can be written as:

$$\sum_j Q_j \int_{T_0}^{T_{out}} C_{p_j} dT - \sum_i Q_i \int_{T_0}^{T_{in}} C_{p_i} dT + \sum_j Q_j \Delta H_f^0(j) - \sum_i Q_i \Delta H_f^0(i) + P_{loss} = 0 \quad (2)$$

where i concerns the reactants and j the products, Q is the molar flowrate, C_p the molar heat capacity and ΔH_f^0 the formation enthalpy of products and reactants. P_{loss} is the heat loss through the wall of the reactor. T_{in} and T_{out} are respectively the inlet and outlet temperatures and T_0 is the reference temperature.

The oxygen inlet flowrate is adjusted to close the energy balance of the system and is the main result of the calculation. From this flowrate, the Equivalent Ratio (ER) which is defined as the ratio between the inlet O₂ flowrate and the O₂ flowrate needed for complete combustion of biomass can be calculated. Results are given in Table 2 for three levels of steam addition and with N₂ or CO₂ as carrier gas in the biomass feeding line, whose flowrates were calculated as described above.

As expected, the required O₂ to reach 1500 °C increases with the addition of steam, by about 18% when 0.64 g of steam per gram of dry biomass is added. The increase does not depend on carrier gas (CO₂ or N₂).

Table 3

Test conditions in the drop tube reactor.

Oxidizing reactant injected	Air flow rate (NL/min)	ER	H ₂ O flow rate (NL/min)	H ₂ O/biomass (g/g db)	CO ₂ flow rate (NL/min)	CO ₂ /biomass (g/g db)
Pyrolysis experiments	–	–	–	–	–	–
Oxygen	1	0.24	–	–	–	–
	1.8	0.44	–	–	–	–
	2.5	0.61	–	–	–	–
Steam (H ₂ O-experiments)	–	–	0.62	0.55	–	–
Carbon dioxide (CO ₂ -experiments)	–	–	–	–	0.4	0.87

With these calculations, the operating conditions of an EFR fed with biomass are specified. They were used to choose the test conditions in the DTR, which are presented in the following section.

2.6.2. Experimental conditions in the DTR

In this study, four different temperatures were selected: 800 °C, 1000 °C, 1200 °C and 1400 °C. Total inlet gas flowrates were respectively 18.8 NL/min, 15.3 NL/min, 13.7 NL/min and 12.1 NL/min, in order to keep a constant gas mean residence time of 4.3 s. In all tests, the wet biomass feeding rate was 1 g/min.

Different atmospheres were studied: inert (N₂) and oxidative with O₂, H₂O and CO₂ as added reactants. The experimental conditions are listed in Table 3 and are related to the preliminary calculation results (Table 2). Our drop tube reactor is designed for small biomass feeding rates and for working in diluted conditions (the dilution gas was nitrogen). So it was impossible to find operating conditions which allow reproducing both reactants/biomass mass ratio and composition of inlet gas of an EFR. Here, the reactant/biomass mass ratio was kept as representative as possible of an EFR.

Several experimental conditions are out of the ranges calculated previously because of technical limitations of the experimental facility. Experiments were conducted at the four temperatures for each reactive atmosphere.

3. Modelling

The experiments were simulated using a numerical model named GASPARG. It was previously adapted and validated to model pyrolysis and steam gasification of biomass in a DTR at high temperature [10]. The GASPARG model having been previously described in [10], only a global description is given. A focus is then made on the chemical reaction modelling, which has been modified.

3.1. The GASPARG model

The GASPARG model is a 1-D model describing biomass gasification in the DTR. It takes into account different phenomena as particle heating, particle drying, pyrolysis reaction, gas phase reactions and char gasification. The differential equations related to gas, tar and soot production and reaction in the gas phase are calculated with CHEMKIN. Then the differential system is solved with LSODE solver which is appropriate for stiff system.

The major hypotheses of GASPARG are:

- The drop tube reactor is modelled as a plug flow reactor.
- The particles are supposed to be spherical.
- Temperature and concentrations are supposed to be uniform inside the particles.

The slip velocity between particles and gas is taken into account. The slip velocity is calculated by Eq. (3) [19] with the drag

Table 4
Biomass and residue composition in pyrolysis reaction in GASPAR.

Biomass composition		
<i>x</i>	<i>y</i>	<i>z</i>
6	8.21	4.08
Residue composition		
<i>s</i>	<i>u</i>	<i>v</i>
1.2 E ⁻³	1.45 E ⁻³	0.2405

coefficient correlation from [20], given in Eq. (4). The model takes into account the modifications of the particle characteristics during the pyrolysis reaction, namely the particle bulk density ρ_p and the particle equivalent spherical diameter d_{es} .

$$\frac{dv_{slip}}{dt} = \frac{(\rho_p - \rho_g)}{\rho_p} g - \frac{3}{4} C_d \frac{\rho_g}{\rho_p} \frac{1}{d_{es}} v_{slip}^2 \quad (3)$$

$$C_d = 1.5 \left[\frac{24}{Re_p} \left(1 + 0.173 Re_p^{0.657} \right) + \frac{0.413}{1 + 16,300 Re_p^{-1.09}} \right] \quad (4)$$

This slip velocity model has been validated with experimental particle velocity measurement [19].

3.2. Pyrolysis

Particle pyrolysis is modelled by a one-step reaction where biomass is decomposed into gas, tar and char. The kinetic of pyrolysis reaction follows an Arrhenius law given in Eq. (5).

$$\begin{aligned} \frac{dm_{dry\ biomass}}{dt} &= -m_{dry\ biomass} k_{pyro} \\ &= -m_{dry\ biomass} A_{pyro} \exp\left(-\frac{E_{a_{pyro}}}{RT}\right) \end{aligned} \quad (5)$$

Kinetic parameters were adjusted so that simulation results fit with experimental results obtained for biomass pyrolysis at 800 °C in a DTR similar to the one used for this study [19].

The pyrolysis reaction for dry ash free biomass is represented by:

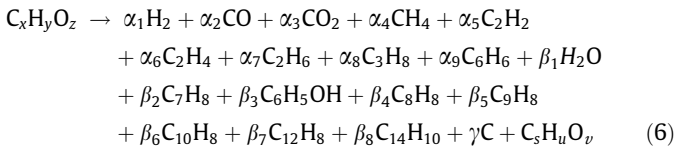


Table 5
Coefficients of pyrolysis reaction in GASPAR.

Formula	Name	Coefficient in Eq. (6)	Value
H ₂	Hydrogen	α_1	0.753
CO	Carbon monoxide	α_2	2.192
CO ₂	Carbon dioxide	α_3	0.347
H ₂ O	Steam	β_1	0.926
CH ₄	Methane	α_4	0.566
C ₂ H ₂	Acetylene	α_5	0.059
C ₂ H ₄	Ethylene	α_6	0.256
C ₂ H ₆	Ethane	α_7	0.0231
C ₃ H ₈	Propane	α_8	0.0153
C ₆ H ₆	Benzene	α_9	0.0391
C ₇ H ₈	Toluene	β_2	0.0326
C ₆ H ₅ OH	Phenol	β_3	0.0243
C ₈ H ₈	Styrene	β_4	0.0164
C ₉ H ₈	Indene	β_5	0.0169
C ₁₀ H ₈	Naphthalene	β_6	0.0286
C ₁₂ H ₈	Acenaphthylene	β_7	0.0042
C ₁₄ H ₁₀	Phenanthrene	β_8	0.0021
C	Char	γ	0.9161

Table 6
Kinetic parameters reactions leading to soot formation.

	Eqs. (7) and (8)	Eq. (9)
Ea (J mol ⁻¹)	167 × 10 ³	41.8 × 10 ³
A (s ⁻¹)	5 × 10 ⁶	2.5 × 10 ⁸

Stoichiometric parameters of the reaction come from pyrolysis experimental result at 800 °C in the DTR. Light gas and benzene coefficients (α_i) were directly fitted on experimental results. Steam and tar compound coefficients (β_i) were adjusted to fill the mass balance, keeping the same tar mixture composition as the one determined by the tar protocol in pyrolysis experiment at 800 °C. The residue C_sH_uO_v, which corresponds to unidentified compounds, represents only 2.5 wt% of initial dry biomass. This residue is considered not to participate in any reaction. In this reaction char is assumed to be pure carbon. A single set of stoichiometric parameters was used for all simulations (Tables 4 and 5).

3.3. Gas phase reactions

In order to improve the prediction capability of the model, the gas phase reactions were modelled using a detailed kinetic scheme. The Ranzi and co-workers kinetic scheme (176 species, 5988 reactions) [16] was selected for gas phase modelling. It is a detailed/lumped mechanism of the pyrolysis, partial oxidation and combustion of Primary Reference Fuels. It takes into account all the tars used here in the global pyrolysis reaction. It was validated in relevant experimental conditions and it predicts PAH formation up to C₂₀ which is convenient for the soot formation modelling [21]. Main studies dealing with this chemical mechanism were conducted on benzene in pyrolysis, partial oxidation and combustion conditions [22], on cyclopentadiene pyrolysis with a focus on the PAH formation [23], on heavy *n*-alkanes (*n*C₇H₁₆, *n*C₁₀H₂₂, *n*C₁₂H₂₂, *n*C₁₆H₃₄) in pyrolysis, partial oxidation and combustion conditions [16].

Soot formation, which is not described in the detailed chemical scheme, is modelled here following a simple reaction pathway including two reactions for soot inception using heavy tars C₂₀H₁₀ and C₂₀H₁₆ and one reaction of soot growth with C₂H₂.



Each reaction is supposed to follow a first order Arrhenius law. The same activation energy as that obtained by Ziegler [24] and used by Septien [10] is used for the inception reactions, while the activation energy for soot particle growth is taken from [25]. The pre-exponential factors were adjusted to fit the experimental data and are presented in Table 6.

3.4. Char gasification

Both char gasification reactions with steam and carbon dioxide are taken into account. Temperature and oxidant concentrations are supposed to be homogeneous in the whole particle. The reactions are supposed to follow Arrhenius laws and the reactive surface of char is supposed to decrease homogeneously in the particle following a Volume Reaction Model:

$$\begin{aligned} \frac{dX}{dt} &= k(T, P_{H_2O})f(X) + k(T, P_{CO_2})f(X) \\ &= \left(A_{H_2O} \exp\left(-\frac{E_{a_{H_2O}}}{RT}\right) P_{H_2O}^{n_{H_2O}} + A_{CO_2} \exp\left(-\frac{E_{a_{CO_2}}}{RT}\right) P_{CO_2}^{n_{CO_2}} \right) (1-X) \end{aligned} \quad (10)$$

Table 7
Kinetic parameters of char gasification by H₂O and CO₂.

	H ₂ O	CO ₂
E _a (J mol ⁻¹)	132.1 × 10 ³	141.3 × 10 ³
A (s ⁻¹ bar ⁻ⁿ)	254 × 10 ³	218.3 × 10 ³
n	1	0.683

P_i is the partial pressure of i in the particle, T is the temperature in the particle, A_i , E_{a_i} and n_i are the kinetic parameters of char gasification by oxidant i ($i = \text{CO}_2$ and H_2O), and X is the char conversion (Eq. (11)).

$$X = 1 - \frac{m(t)}{m(t=0)} \quad (11)$$

with $m(t)$, the mass of char at time t .

Gasification kinetic parameters were optimized to fit the experimental mass of char measured at the end of experiments. Experimental results used to optimize the kinetic parameters are presented in Fig. A1 in supplementary data. These experiments were conducted at 4 different temperatures – 800, 1000, 1200 and 1400 °C – in three different atmospheres: inert, and with addition of H₂O and CO₂ (Table 3). The set of fitted parameters is presented in Table 7.

These sets of parameters are relevant compared to the results given in literature for woody biomass gasification [26]. However, gasification can be limited by the diffusive transfer in particle at high temperature [6], which is thus included in the optimized parameters.

Note that the oxidation of solids (char and soot) by O₂ was not taken into account in the model. This choice will be discussed in the following of the text. Moreover, soot gasification by steam and CO₂ is neglected. Indeed, soot gasification experiments have shown that soot gasification by steam was 2–20 times slower than char gasification between 750 °C and 950 °C [27]. Soot gasification by CO₂ is 2–30 times slower than char gasification at 1100 °C [28].

4. Results and discussion

Both experimental and simulation results are presented and discussed in this section. First, the influence of presence of steam and CO₂ on biomass gasification is studied by comparison with pyrolysis experiments, whose results are not detailed here as they

are similar to those found in the same facility by Septien [10]. Then the influence of O₂ is detailed and discussed.

4.1. Influence of steam or CO₂ addition

The influence of the addition of H₂O or CO₂ on carbon conversion into gas, char and remaining products (soot and tar) is discussed first. Then the gas composition is detailed. At last, the simulation results are used to better understand the influence of the addition of H₂O or CO₂ on tar and soot production.

4.1.1. Distribution of carbon in products

The goal of the gasification being to produce a maximum of CO and H₂, it is interesting to study the carbon repartition in gas, char and tar + soot. In this section we define the carbon conversion into gas as the ratio between the mass of carbon in the analyzed gas (CO, CO₂, CH₄, C₂H₂, C₂H₄, C₂H₆, C₃H₈ and C₆H₆) and the mass of carbon coming from biomass. Thus the carbon added by CO₂ injection in CO₂-experiments is subtracted. The expression of carbon conversion into gas is given in Eq. (12).

$$\text{Carbon conversion} = \frac{m_{\text{C-gas analyzed}} - m_{\text{C-CO}_2\text{in}}}{m_{\text{C-biomass}}} \quad (12)$$

The fraction of carbon in char is calculated from char yield and carbon content of char (about 80 wt%). Finally the remaining carbon, attributed to soot and tars, is calculated to fill the carbon balance.

Carbon distribution in gas, char and in tar + soot products is given in Fig. 3 as a function of temperature.

The addition of oxidant (H₂O or CO₂) has a significant influence on carbon distribution especially at 1200 and 1400 °C. The conversion of carbon into gas in pyrolysis experiments reaches a maximum at 1000 °C (67% of carbon from initial biomass) and remains constant between 1200 and 1400 °C. In H₂O and CO₂-experiments the maximum is reached at 1400 °C with respectively 77% and 71% of carbon from initial biomass. The simulation gives a good prediction of carbon conversion into gas even if the calculation overestimates the carbon conversion at 1000 °C.

The carbon fraction into char decreases as temperature increases. This is attributed to char gasification reaction. Addition of steam or CO₂ has a significant influence on char consumption at 1200 °C and 1400 °C. Altogether the model with fitted kinetic parameters allows a good representation of char consumption in function of temperature and reproduces very satisfactorily the influence of H₂O and CO₂.

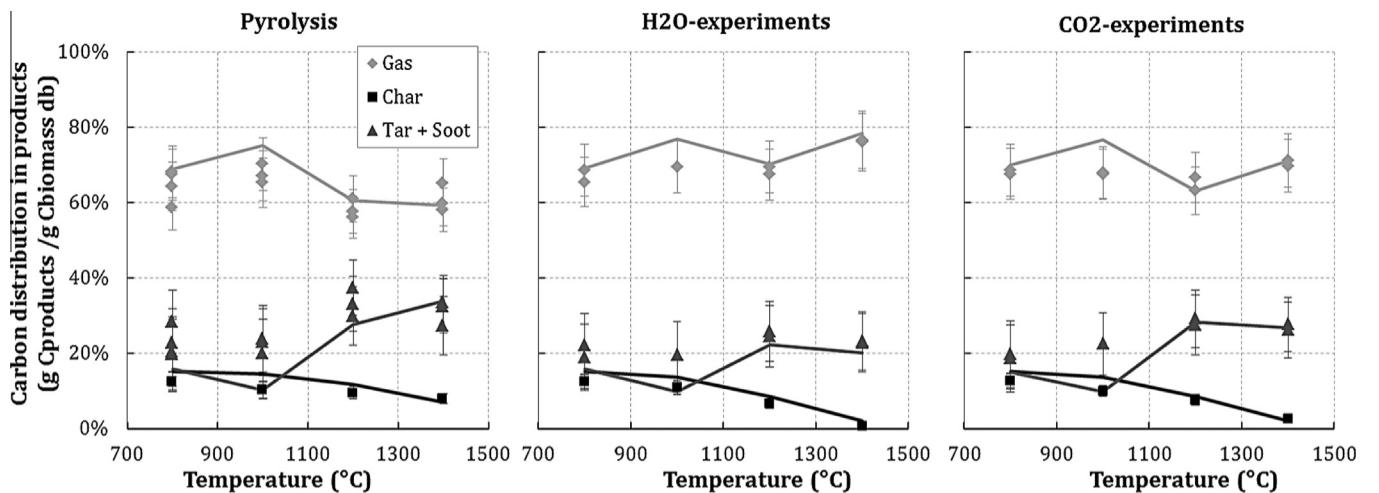


Fig. 3. Carbon distribution in gas, char and tar + soot in pyrolysis, H₂O and CO₂-experiments – experimental results (dots) and simulation results (lines).

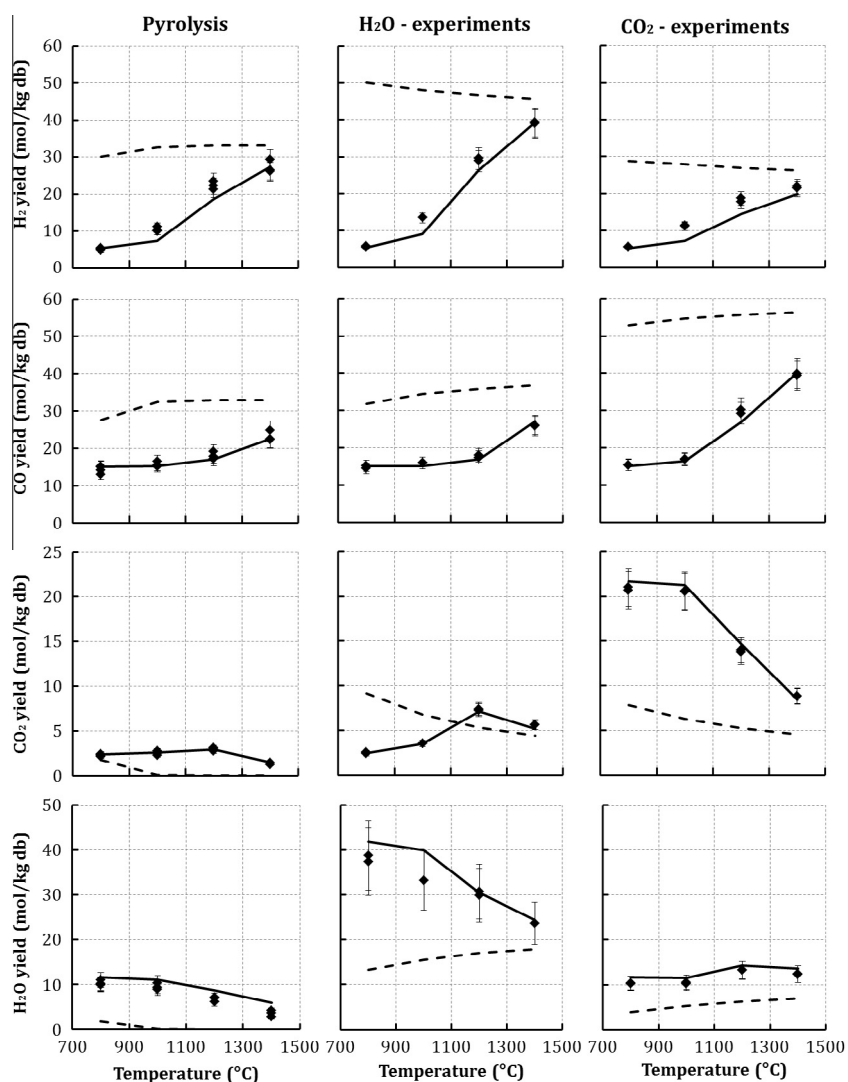


Fig. 4. H₂, CO, CO₂ and H₂O yields as a function of temperature in pyrolysis, H₂O and CO₂-experiments – experimental results (dots), simulation results (continuous lines) and thermodynamic equilibrium results (dotted lines).

The fraction of carbon in soot and tars determined from experiments seems to remain constant between 800 and 1000 °C, and then increases to reach a plateau between 1200 and 1400 °C. This could be explained by two opposite phenomena: the tar yield decreases when temperature increases because of cracking reactions, whereas soot production increases with temperature. Indeed, previous works show that tar contents are very low above 1000 °C [7,10] while soot production is significant at 1000 °C and above [4]. The presence of steam or CO₂ leads to a decreasing amount of carbon in tar and soot, certainly because of soot precursors consumption, which is discussed in more details in Section 4.1.3. The simulation allows well reproducing the carbon distribution except at 1000 °C where carbon conversion into gas is overestimated and carbon in tar and soot is underestimated.

4.1.2. Gas species yields

The experimental and simulated gas species yields, as well as those at thermodynamic equilibrium, are shown as a function of temperature in Fig. 4 and Fig. A2 in supplementary data. Note that gas yields include the H₂O or CO₂ addition.

In all experiments, H₂, CO, H₂O, CO₂ and CH₄ are the major gas species, followed by C₂H₂, C₂H₄, C₆H₆, C₂H₆ and C₃H₈. H₂ and CO

yields always increase with temperature. H₂O yield decreases as temperature increases except in CO₂-experiments in which it slightly increases. The variation of CO₂ yield depends on experimental conditions: in pyrolysis experiments CO₂ yield is steady with temperature until 1200 °C and then decreases, while in H₂O-experiments it increases until 1200 °C and then decreases; in CO₂-experiments the CO₂ yield is steady between 800 and 1000 °C and then strongly decreases.

Influence of addition of H₂O or CO₂ on CO and H₂ yields is notable above 1000 °C. At 1200 and 1400 °C, H₂ yield decreases in CO₂-experiments and increases in H₂O-experiments while CO yield increases in CO₂-experiments.

For light hydrocarbons (CH₄, C₂H₂, C₂H₄, C₂H₆ and C₃H₈) and benzene, the addition of CO₂ or H₂O has no significant influence even at high temperature. In our operating conditions, the steam reforming and vapo-cracking reactions of light hydrocarbons are not significantly enhanced by the steam addition. In all conditions, the results of the tests and of the model are different from the predictions at thermodynamic equilibrium. The model allows reproducing the major gas yields with a very good accuracy (relative error < ±20% in most cases). The maximal deviations are obtained for H₂ yields at 1000 °C and steam yield at 1400 °C in pyrolysis

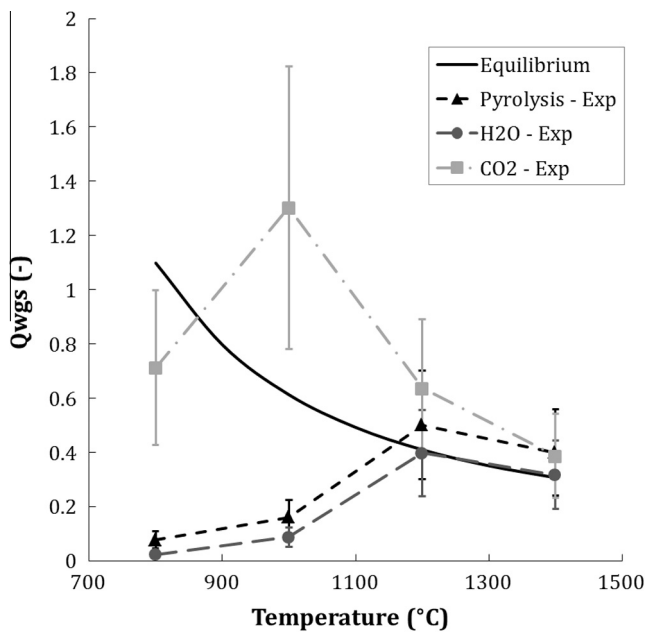


Fig. 5. Water-gas-shift constants from pyrolysis, H₂O and CO₂-experiments and at thermodynamic equilibrium as a function of temperature.

experiments. Simulation also accurately predicts CH₄ and C₂H₂ yields in the whole range of temperature (Fig. A2 in supplementary data). However, C₂H₄ production is overestimated at 800, 1000 and 1200 °C. In spite of these slight differences the tendencies are always well reproduced, which is very satisfying.

According to the previous observations, H₂O or CO₂ addition mainly influences H₂, CO, H₂O and CO₂ yields, at 1200 and 1400 °C only. Three global phenomena could lead to this result: char gasification, tar and soot gasification, and water-gas shift reaction (Eq. (13)).



The two first phenomena lead to an increase of H₂ and CO yields. However, as noticed before, at 1200 and 1400 °C, in CO₂ experiments, the H₂ yield is lower than in pyrolysis experiments, while in H₂O experiments, the CO yield hardly increases compared

to pyrolysis. This should be due to the third phenomenon mentioned above: the water-gas shift reaction. The water-gas shift constants calculated from experimental results and at thermodynamic equilibrium are given in Fig. 5 for each condition.

As shown in Fig. 5, the water-gas shift reaction is at thermodynamic equilibrium at 1200 and 1400 °C, whatever the atmosphere. This reaction then controls the relative H₂, CO, CO₂ and H₂O contents.

4.1.3. Soot and tar yields

The soot and tar yields cannot be precisely measured in experiments and we only have a qualitative estimation by direct observation. The GASPARG model shows a good ability to predict the gas and char yields, thus it is used here to investigate the influence of temperature and H₂O and CO₂ on soot and tar yields. Fig. 6(a) represents the soot yields calculated with GASPARG.

A high soot yield (between 0.1 and 0.17 kg/kg biomass db) is predicted at 1200 and 1400 °C as observed in experiments. The presence of steam decreases the soot yield although no soot gasification reactions are taken into account in the model. Steam or radicals derived from steam could react with soot precursors. Liu et al. [29] show that major chemical effect of addition of steam on soot formation inhibition is due to OH formation which is responsible for soot precursors decrease. The influence of CO₂ is lower but significant at 1400 °C. CO₂ only has a slight chemical effect on soot inhibition by enhancing OH formation [30]. In our case, H₂O produced by RWGS reaction is certainly also responsible for the inhibition of soot formation in CO₂-experiments.

Let us remind that the tar compounds are defined here as the compounds heavier than benzene. The GASPARG predicted tar yields are given in Fig. 6(b). The main compounds predicted by GASPARG are Polyaromatic Hydrocarbons (PAH): naphthalene, indene, styrene, acenaphthylene, phenanthrene, pyrene and C₂₀ species. The tar yield decreases when temperature increases because of PAH cracking and soot formation. The presence of oxidant has a very weak influence on tar yields.

In conclusion, the influence of addition of steam or CO₂ on gasification products is rather similar. This influence is only visible at 1200 and 1400 °C. The presence of oxidant then leads to a char conversion increase and a soot formation decrease, which leads to a higher carbon conversion into gas. The gas phase composition is mainly affected by the WGS reaction while light hydrocarbon yields remain unchanged. The GASPARG simulation shows a very satisfying agreement with experimental results.

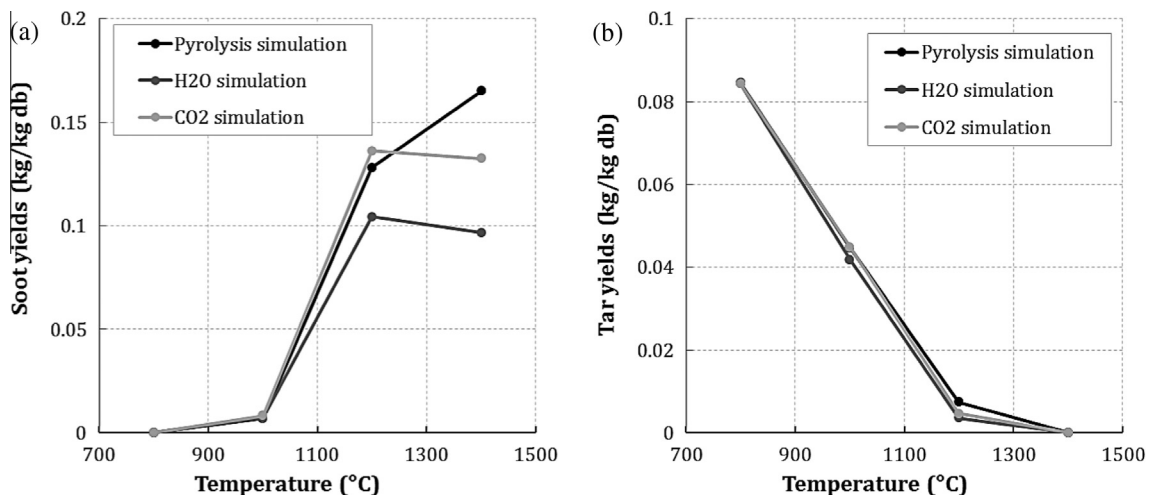


Fig. 6. Soot yields (a) and tar yield (b) as a function of different temperature calculated with GASPARG in pyrolysis, H₂O and CO₂-experiments.

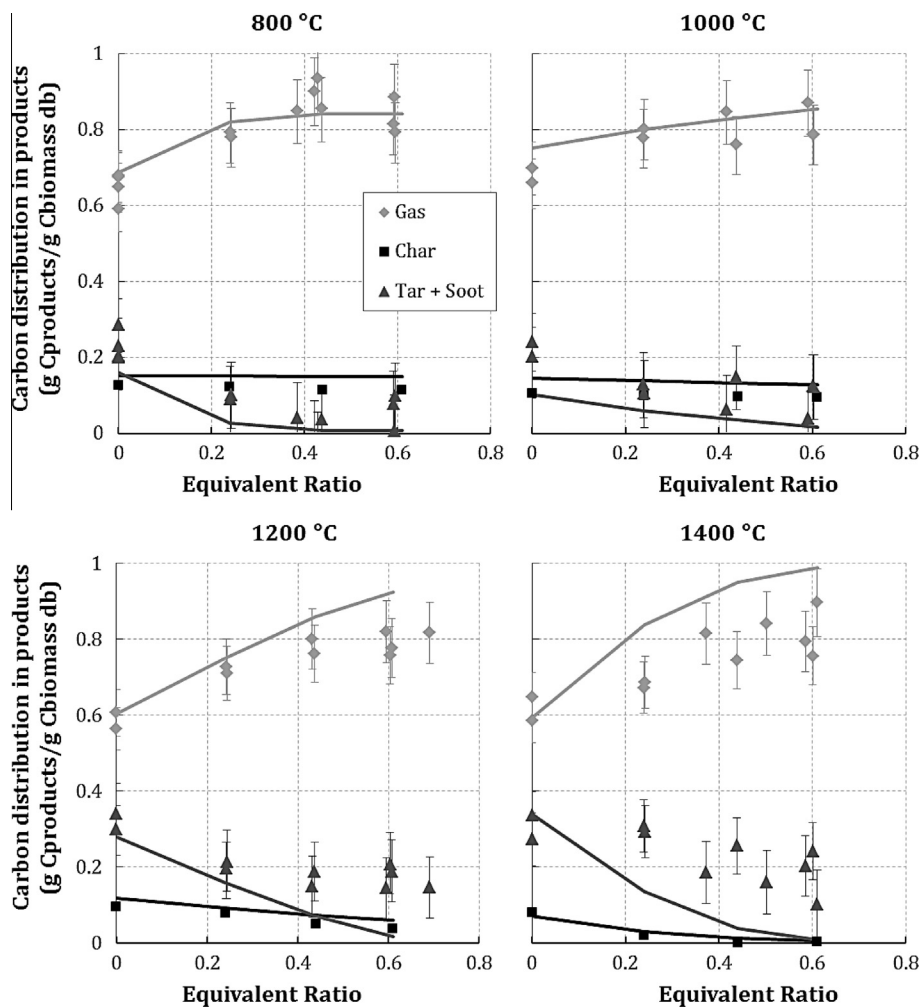


Fig. 7. Carbon distribution in gas, char and tar + soot as a function of ER at 800, 1000, 1200 and 1400 °C – experimental results (dots) and simulation results (lines).

4.2. Influence of O_2

First, the influence of O_2 on carbon distribution is discussed. Then the char and gas yields are presented as a function of ER. At last, the simulation results are used to better understand the influence of the addition of O_2 on tar and soot production.

4.2.1. Distribution of carbon from biomass

The carbon distribution into gas, char and tar + soot are given at each temperature as a function of ER in Fig. 7. Note that tar + soot for experimental results is the remaining part to close the carbon balance.

According to experimental results, carbon conversion into gas increases with ER whatever the temperature and reaches a plateau at about 80–85%. At 800 and 1000 °C, this plateau is due to incomplete char conversion even at ER = 0.61. Indeed, the carbon fraction in char has a minor dependence on ER and remains almost constant at about 10–13%. At 1200 and 1400 °C, the fraction of carbon in char decreases as ER increases and reaches 0% at 1400 °C and ER = 0.61. The plateau can only be explained by production of tar and soot. We know that tars are converted at these temperatures thus the remaining part of carbon – around 20% – mainly comes from soot which are produced at high temperature. However, we have found out that only a very small quantity of soot, which cannot represent 20% of input carbon, was produced for the tests at 1400 °C with ER of 0.44 and 0.61. Additional tests were performed

to check the experiment repeatability, confirming the same inconsistency. The soot yield being obtained by difference of the carbon balance, we think that this discrepancy could come from an error in the measurement of gas yields in these conditions.

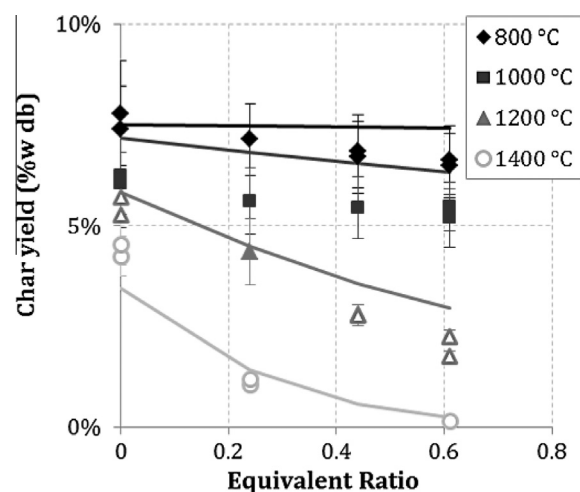


Fig. 8. Char yields as a function of ER at 800, 1000, 1200 and 1400 °C – experimental results (dots) and simulation results (lines) – char ash content measured in furnace (full dots) and in TGA (empty dots).

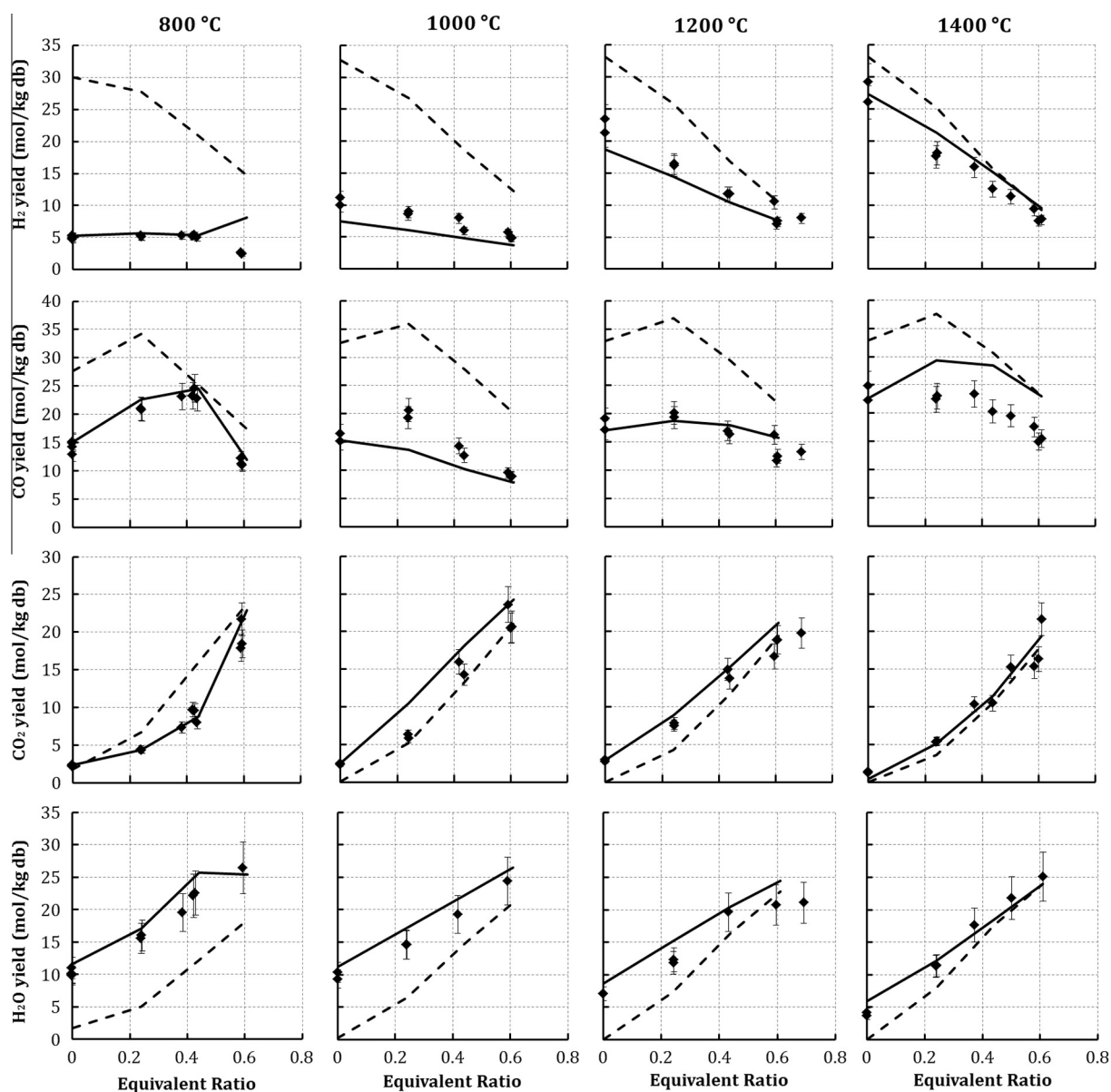


Fig. 9. H₂, CO, CO₂ and H₂O yields as a function of ER at 800, 1000, 1200 and 1400 °C – experimental results (dots), simulation results (continuous lines) and thermodynamic equilibrium results (dotted lines).

The simulation results are in very good agreement with experimental ones in all conditions at 800 and 1000 °C, and for the lower values of ER at 1200 and 1400 °C. The conversion of carbon into gas predicted by the model is higher than the one determined from the experiments in the other cases.

To conclude this section, at 800 and 1000 °C the conversion of carbon into gas is limited by a significant fraction of carbon in unconverted char, while at 1200 and 1400 °C, soot seems to be responsible for the carbon gasification limitation. In the next section, the char yield evolution with ER and temperature is detailed.

4.2.2. Char yield

The char mass yields are given in Fig. 8 as a function of ER at different temperatures.

Experimental and simulation results both show that char yield decreases as temperature increases whatever the ER, because of gasification reaction enhancement. It also decreases as ER

increases even if the influence of ER is smaller at 800 and 1000 °C than at 1200 and 1400 °C.

The GASPARG model gives a satisfying prediction of char yields, especially at 1200 and 1400 °C. Let us remind that it takes into account char gasification by steam and CO₂ but not direct combustion of char (Section 3.4). The kinetic parameters of the gasification reactions were not fitted with these experimental results, but only with those obtained with addition of H₂O and CO₂. The good agreement between these experimental and modelling results suggests that in our reactor and in these operating conditions, the char combustion is negligible. The O₂ and char yields profiles calculated with GASPARG along the reactor show that when char is produced – at the end of pyrolysis reaction – no oxygen remains to combust char. Thus the char yield decrease as ER increases would only be due to the increase of steam and CO₂ partial pressures, H₂O and CO₂ being produced by the combustion of a part of tars and gas species. The gas yields and gas phase reactions are discussed in the next section.

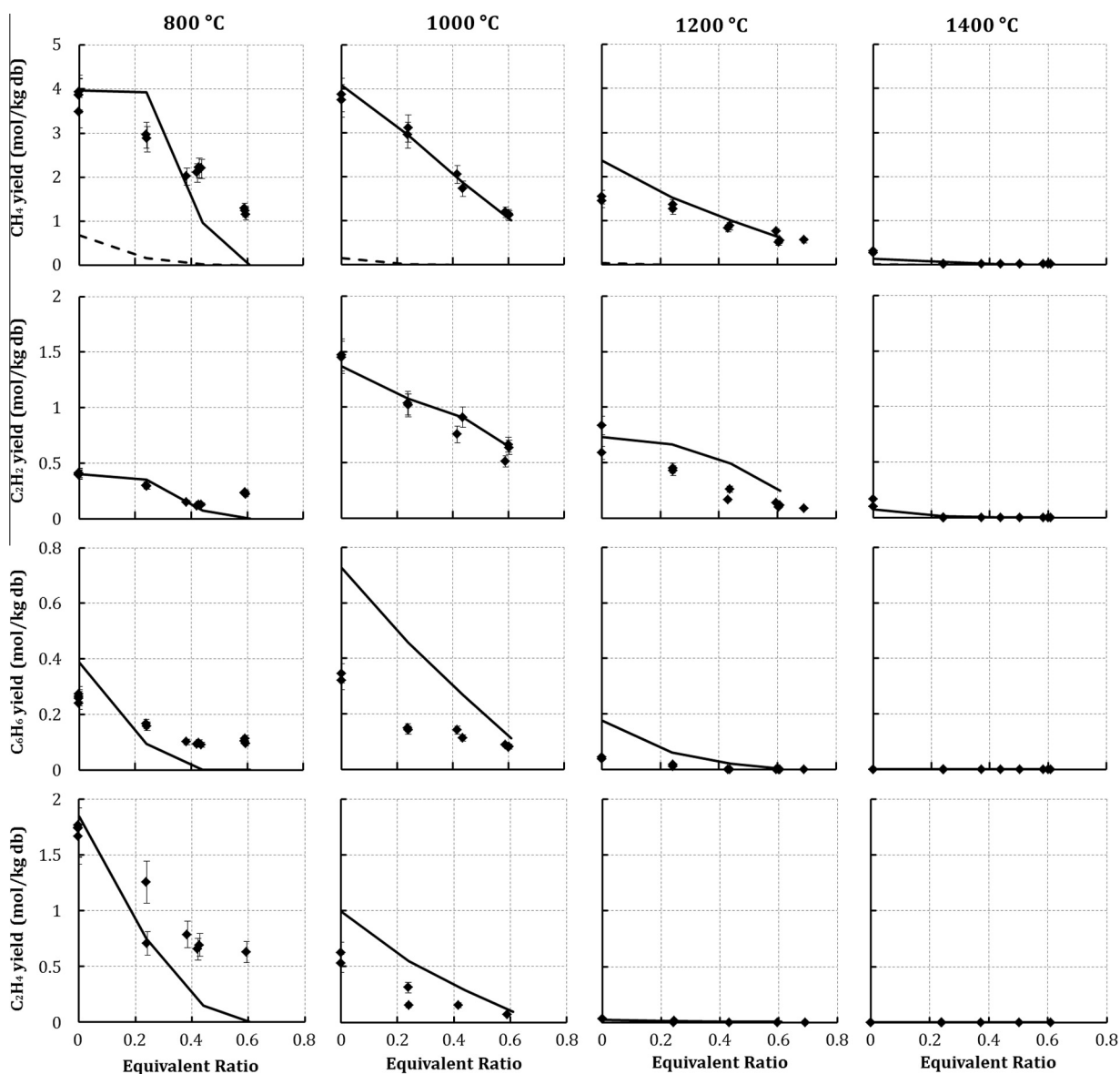


Fig. 10. CH₄, C₂H₂, C₆H₆ and C₂H₄ yields as a function of ER at 800, 1000, 1200 and 1400 °C – experimental results (dots), simulation results (continuous lines) and thermodynamic equilibrium results (dotted lines).

4.2.3. Gas species yields

Experimental and simulated gas species yields, together with predictions at thermodynamic equilibrium, are presented in function of ER at different temperatures in Figs. 9 and 10.

The experimental results show that at each temperature, H₂ yield decreases as ER increases, which is probably due to its oxidation. CO₂ and H₂O yields increase with ER at all temperatures, because they are final combustion products. At 800 and 1000 °C, the CO yield first increases with ER to reach a maximum for ER ranging between 0.2 and 0.4, depending on the temperature. At 1200 °C and 1400 °C, the CO yield decreases first slightly, and then more rapidly as ER increases. The minimum of CO yield is always measured at ER = 0.61 whatever the temperature. This behaviour is certainly due to two competitive phenomena. At low ER, CO is produced by partial combustion of hydrocarbons while at higher ER it is also partially oxidized. All hydrocarbon gas yields decrease as ER increases because of combustion reactions.

Simulation globally gives rather good predictions of gas yields and confirms our explanations on the evolution of gas yields with

ER. Except from the cases with ER equal to 0.4 and 0.61 at 1400 °C, the results of our model differ from the calculations at thermodynamic equilibrium. So in all other cases, reaction kinetics have a significant influence on the product yields at the reactor output. If we look at the gas composition along the reactor with GASPARG, both tar and gas are burnt. Indene, naphthalene, toluene, and styrene are burnt first, followed by phenanthrene, acenaphthylene and benzene and at last by methane, acetylene, di-hydrogen and carbon monoxide. Note that for temperatures of 1000 °C and higher, gas combustion kinetic rates are higher than pyrolysis one, and all hydrocarbons released in pyrolysis are burnt as soon as they are formed, as long as some O₂ is still present in the reactor. So soot particles can only be formed in the lower part of the reactor, where no O₂ remains. This confirms our choice not to consider direct oxidation of soot particles in the model, which would not have modified the results. At high temperature, CO and H₂ are also produced by the WGS reaction which reaches thermodynamic equilibrium at the end of the reactor. At 800 °C in presence of oxygen, light hydrocarbons yields are generally underestimated while H₂

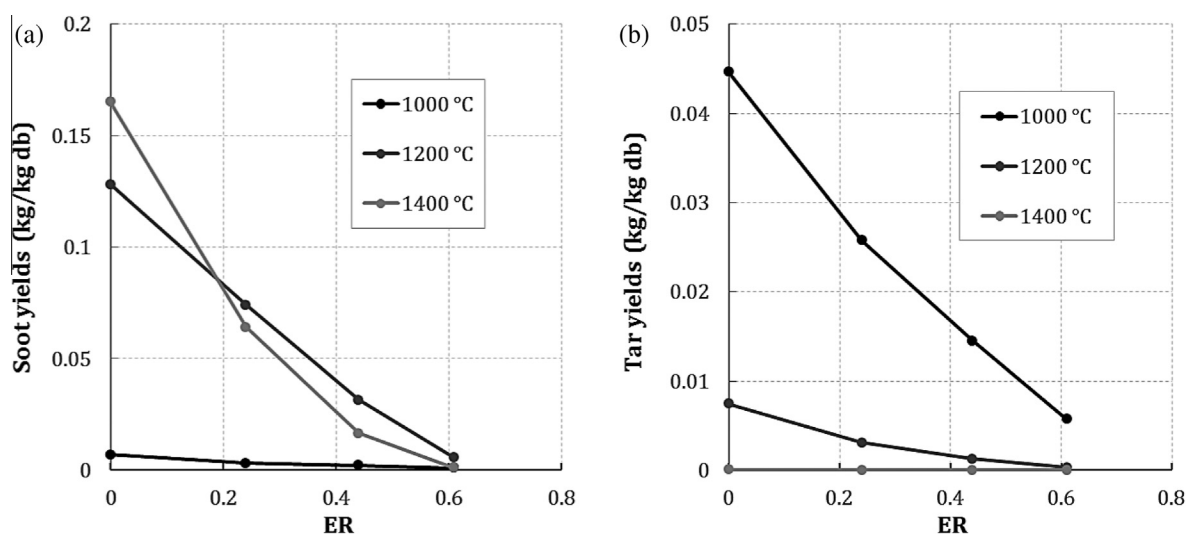


Fig. 11. Soot (a) and tar yields (b) calculated with GASPAP as a function of ER at different temperature.

yield is overestimated at ER = 0.61. This seems to be due to a too long delay between pyrolysis reaction and ignition of pyrolysis gas. CO yields are not so well represented especially at 1000 °C where CO yields are underestimated and at 1400 °C where they are overestimated. To conclude, GASPAP model allows a satisfying prediction of gases above 800 °C. Based upon this, we use it to investigate soot and tar yields in the next section.

4.2.4. Soot and tar yields

Influence of oxygen on soot and tar yields is studied with simulation results given by GASPAP. Soot yields are given in Fig. 11(a) as a function of ER.

O₂ addition has a strong influence on predicted soot yield which decreases as ER increases. As expected the maximum yields are found at 1200 °C and 1400 °C. It was previously discussed that soot yields at 1400 °C and 1200 °C at ER = 0.61 are certainly underestimated even if the decrease in soot production was experimentally observed. As mentioned previously, no soot combustion or gasification reaction is included in the model. Decrease of soot yield can only be due to consumption of soot precursors.

Tar yield as a function of ER at different temperature is given in Fig. 11(b). As expected, increase of ER decreases the tar yield and no tar are predicted at 1400 °C. In Section 4.1, we put into evidence that addition of H₂O and CO₂ has no influence on tar yield in the model. Considering that the ranges of CO₂ and steam concentration are similar, tar yield decrease is thus only due to direct combustion of tar. Tar being soot precursors, the soot decrease is mainly due to tar burning.

5. Conclusion

Both experiments in a drop tube furnace and simulation with the GASPAP model enabled to study the influence of H₂O, CO₂ and O₂ addition on gasification products in an entrained flow reactor. The work was conducted in representative conditions of an entrained flow reactor: oxidant/biomass ratio, temperature, particle size and residence time.

The GASPAP model was improved with (1) a new pyrolysis global reaction, which takes into account the main tars produced, (2) a more efficient gas phase model which allows predicting heavy tars until C₂₀, (3) two fitted gasification laws to take into account the influence of both H₂O and CO₂ and (4) a simple soot formation mechanism. The model is validated on the whole range of experimental conditions and generally allows a good prediction

of gas and char yields as well as relevant evolution of soot and tar yields. It can be used for predictive calculations taking the obvious precautions in the use of calculation results. It also enables to investigate the detailed kinetics pathways responsible for the formation of problematic species in EFR process as soot, methane, and char.

Char yield decrease as ER increases can be very well predicted accounting for char gasification by H₂O and CO₂ only. This lets us think that char oxidation by O₂ is negligible in our conditions. Similarly, soot yield decrease as ER increases is predicted by GASPAP taking into account neither direct combustion nor steam gasification of soot. The soot precursors certainly react with OH radicals which stops soot inception.

In typical process conditions in an EFR –1400 °C and ER = 0.44 – char is almost completely gasified and only a small amount of soot (2 wt% db) is produced. Considering the steam and CO₂ influence, their addition seems unnecessary. Indeed it could lower a bit the soot production but it will certainly also decrease the energy yield of the process.

Appendix A. Supplementary material

Supplementary data associated with this article can be found, in the online version, at <http://dx.doi.org/10.1016/j.fuel.2015.10.046>.

References

- [1] International Energy Agency. World energy outlook 2010. Paris: International Energy Agency; 2010.
- [2] Stocker TF, editor. Intergovernmental panel on climate change. Climate change 2013 the physical science basis; working group I contribution to the fifth assessment report of the intergovernmental panel on climate change. New York (NY): Cambridge Univ. Press; 2014.
- [3] Bitowft B, Andersson LA, Bjerle I. Fast pyrolysis of sawdust in an entrained flow reactor. Fuel 1989;68:561–6. [http://dx.doi.org/10.1016/0016-2361\(89\)90150-6](http://dx.doi.org/10.1016/0016-2361(89)90150-6).
- [4] Qin K, Jensen PA, Lin W, Jensen AD. Biomass gasification behavior in an entrained flow reactor: gas product distribution and soot formation. Energy Fuels 2012;26:5992–6002. <http://dx.doi.org/10.1021/ef300960x>.
- [5] Zhang Y, Kajitani S, Ashizawa M, Miura K. Peculiarities of rapid pyrolysis of biomass covering medium- and high-temperature ranges. Energy Fuels 2006;20:2705–12. <http://dx.doi.org/10.1021/ef060168r>.
- [6] Septien S, Valin S, Dupont C, Peyrot M, Salvador S. Effect of particle size and temperature on woody biomass fast pyrolysis at high temperature (1000–1400 °C). Fuel 2012;97:202–10. <http://dx.doi.org/10.1016/j.fuel.2012.01.049>.
- [7] Zhang Y, Kajitani S, Ashizawa M, Oki Y. Tar destruction and coke formation during rapid pyrolysis and gasification of biomass in a drop-tube furnace. Fuel 2010;89:302–9. <http://dx.doi.org/10.1016/j.fuel.2009.08.045>.

- [8] Zhou J, Chen Q, Zhao H, Cao X, Mei Q, Luo Z, et al. Biomass-oxygen gasification in a high-temperature entrained-flow gasifier. *Biotechnol Adv* 2009;27:606–11. <http://dx.doi.org/10.1016/j.biotechadv.2009.04.011>.
- [9] Couhert C, Salvador S, Commandré J-M. Impact of torrefaction on syngas production from wood. *Fuel* 2009;88:2286–90. <http://dx.doi.org/10.1016/j.fuel.2009.05.003>.
- [10] Septien S, Valin S, Peyrot M, Spindler B, Salvador S. Influence of steam on gasification of millimetric wood particles in a drop tube reactor: experiments and modelling. *Fuel* 2013;103:1080–9. <http://dx.doi.org/10.1016/j.fuel.2012.09.011>.
- [11] Naruse I, Ueki Y, Isayama T, Shinba T, Kihedu JH, Yoshiie R. Reaction characteristic of woody biomass with CO₂ and H₂O. *Tetsu-Hagane J Iron Steel Inst Jpn* 2010;96:151–4.
- [12] Kobayashi N, Tanaka M, Piao G, Kobayashi J, Hatano S, Itaya Y, et al. High temperature air-blown woody biomass gasification model for the estimation of an entrained down-flow gasifier. *Waste Manage* 2009;29:245–51. <http://dx.doi.org/10.1016/j.wasman.2008.04.014>.
- [13] Weiland F, Hedman H, Marklund M, Wiinikka H, Öhrman O, Gebart R. Pressurized oxygen blown entrained-flow gasification of wood powder. *Energy Fuels* 2013;27:932–41. <http://dx.doi.org/10.1021/ef301803s>.
- [14] Ku X, Li T, Løvås T. Eulerian-Lagrangian simulation of biomass gasification behavior in a high-temperature entrained-flow reactor. *Energy Fuels* 2014;28:5184–96. <http://dx.doi.org/10.1021/ef5010557>.
- [15] Norinaga K, Sakurai Y, Sato R, Hayashi J. Numerical simulation of thermal conversion of aromatic hydrocarbons in the presence of hydrogen and steam using a detailed chemical kinetic model. *Chem Eng J* 2011;178:282–90. <http://dx.doi.org/10.1016/j.cej.2011.10.003>.
- [16] Ranzi E, Frassoldati A, Granata S, Faravelli T. Wide-range kinetic modeling study of the pyrolysis, partial oxidation, and combustion of heavy n-alkanes. *Ind Eng Chem Res* 2005;44:5170–83. <http://dx.doi.org/10.1021/ie049318g>.
- [17] Sakurai Y, Yamamoto S, Kudo S, Norinaga K, Hayashi J. Conversion characteristics of aromatic hydrocarbons in simulated gaseous atmospheres in reducing section of two-stage entrained-flow coal gasifier in air- and O₂/CO₂-blown modes. *Energy Fuels* 2013;27:1974–81. <http://dx.doi.org/10.1021/ef301658d>.
- [18] Ranzi E, Corbetta M, Manenti F, Pierucci S. Kinetic modeling of the thermal degradation and combustion of biomass. *Chem Eng Sci* 2014;110:2–12. <http://dx.doi.org/10.1016/j.ces.2013.08.014>.
- [19] Chen L. *Fast pyrolysis of millimetric wood particles between 800 °C and 1000 °C*. Lyon: Génie des Procédés, Université Claude Bernard; 2009.
- [20] Turton R, Levenspiel O. A short note on the drag correlation for spheres. *Powder Technol* 1986;47:83–6. [http://dx.doi.org/10.1016/0032-5910\(86\)80012-2](http://dx.doi.org/10.1016/0032-5910(86)80012-2).
- [21] Saggese C, Sánchez NE, Frassoldati A, Cuoci A, Faravelli T, Alzueta MU, et al. Kinetic modeling study of polycyclic aromatic hydrocarbons and soot formation in acetylene pyrolysis. *Energy Fuels* 2014;28:1489–501. <http://dx.doi.org/10.1021/ef402048q>.
- [22] Saggese C, Frassoldati A, Cuoci A, Faravelli T, Ranzi E. A wide range kinetic modeling study of pyrolysis and oxidation of benzene. *Combust Flame* 2013;160:1168–90. <http://dx.doi.org/10.1016/j.combustflame.2013.02.013>.
- [23] Djokic MR, Van Geem KM, Cavallotti C, Frassoldati A, Ranzi E, Marin GB. An experimental and kinetic modeling study of cyclopentadiene pyrolysis: first growth of polycyclic aromatic hydrocarbons. *Combust Flame* 2014;161:2739–51. <http://dx.doi.org/10.1016/j.combustflame.2014.04.013>.
- [24] Ziegler I. *Modélisation cinétique des dépôts de pyrocarbone obtenus par pyrolyse d'hydrocarbures*. Vandoeuvre-les-Nancy: INPL; 2004.
- [25] D'Anna A, Kent JH. Modeling of particulate carbon and species formation in coflowing diffusion flames of ethylene. *Combust Flame* 2006;144:249–60. <http://dx.doi.org/10.1016/j.combustflame.2005.07.011>.
- [26] Di Blasi C. Combustion and gasification rates of lignocellulosic chars. *Prog Energy Combust Sci* 2009;35:121–40. <http://dx.doi.org/10.1016/j.pecs.2008.08.001>.
- [27] Septien S, Valin S, Peyrot M, Dupont C, Salvador S. Characterization of char and soot from millimetric wood particles pyrolysis in a drop tube reactor between 800 °C and 1400 °C. *Fuel* 2014;121:216–24. <http://dx.doi.org/10.1016/j.fuel.2013.12.026>.
- [28] Qin K, Lin W, Fæster S, Jensen PA, Wu H, Jensen AD. Characterization of residual particulates from biomass entrained flow gasification. *Energy Fuels* 2013;27:262–70. <http://dx.doi.org/10.1021/ef301432q>.
- [29] Liu F, Consalvi J-L, Fuentes A. Effects of water vapor addition to the air stream on soot formation and flame properties in a laminar coflow ethylene/air diffusion flame. *Combust Flame* 2014;161:1724–34. <http://dx.doi.org/10.1016/j.combustflame.2013.12.017>.
- [30] Liu F, Guo H, Smallwood GJ, Gülder ÖL. The chemical effects of carbon dioxide as an additive in an ethylene diffusion flame: implications for soot and NO_x formation. *Combust Flame* 2001;125:778–87. [http://dx.doi.org/10.1016/S0010-2180\(00\)00241-8](http://dx.doi.org/10.1016/S0010-2180(00)00241-8).